Arch. Metall. Mater. **62** (2017), 2B, 993-997

DOI: 10.1515/amm-2017-0140

E.-B. KIM*, J.-M. KOO, S.-J. HONG*#

EFFECT OF Ga_2O_3 NANOPARTICLES DISPERSION ON MICROSTRUCTURE AND THERMOELECTRIC PROPERTIES OF p-TYPE BiSbTe BASED ALLOYS

In this study, p-type $Bi_{0.5}Sb_{1.5}Te_3$ based nanocomposites with addition of different weight percentages of Ga_2O_3 nanoparticles are fabricated by mechanical milling and spark plasma sintering. The fracture surfaces of all $Bi_{0.5}Sb_{1.5}Te_3$ nanocomposites exhibited similar grain distribution on the entire fracture surface. The Vickers hardness is improved for the $Bi_{0.5}Sb_{1.5}Te_3$ nanocomposites with 6 wt% added Ga_2O_3 due to exhibiting fine microstructure, and dispersion strengthening mechanism. The Seebeck coefficient of $Bi_{0.5}Sb_{1.5}Te_3$ nanocomposites are significantly improved owing to the decrease in carrier concentration. The electrical conductivity is decreased rapidly upon the addition of Ga_2O_3 nanoparticle due to increasing carrier scattering at newly formed interfaces. The peak power factor of 3.24 W/mK^2 is achieved for the base $Bi_{0.5}Sb_{1.5}Te_3$ sintered bulk. The $Bi_{0.5}Sb_{1.5}Te_3$ nanocomposites show low power factor than base sample due to low electrical conductivity.

Keywords: Thermoelectric properties, $Bi_{0.5}Sb_{1.5}Te_3$ alloys, Seebeck coefficient, Mechanical alloying, Spark plasma sintering

1. Introduction

Thermoelectric (TE) solid state devices have been developed for power generation and refrigeration cooling applications. The performance of thermoelectric devices is determined by a dimensionless figure of merit, $ZT = \alpha^2\sigma T/\kappa$, where α is the Seebeck coefficient, σ is the electrical conductivity, κ is the thermal conductivity, T is the absolute temperature respectively. The TE materials with high power factor ($\alpha^2\sigma$), and low thermal conductivity (κ) are required to get high figure or merit values [1].

Bismuth-telluride based alloys show exceptional TE properties at ambient temperatures, and employed for commercial TE modules over the fast five decades. These alloys have a narrow energy gap, and can vary the electrical properties by doping. In addition, Bi-Sb-Te based compounds have a rhombohedral crystal structure (space group $R\bar{3}m$), with weak force of van der walls bonding between the successive Te-Te layers, can easily occupied by foreign atoms (modulations) [2,3]. So far, commercial ingots of p-type and n-type Bi-Te based alloys are fabricated by single crystal (zone melting) techniques. However, these conventional processes include complex processing procedures such as high annealing temperature, and difficult to control the exact composition with stoichiometric ratios. In addition, zone melting (ZM) bulks have cleave along the *c*-direction due to weak van der Walls forces between $Te^{(1)}$-$Te^{(1)}$ layers [4]. Recently, powder metallurgy come forward to overcome these problem, and achieved high thermoelectric as well as mechanical properties [5]. Poudel et al. fabricated p-type Bi-Te based alloys with ZT of 1.4 via bulk nanostructuring approach at 400K by ball milling and hot pressing [6]. Xie et al. reported the Bi-Sb-TE ternary alloys with improved thermoelectric performance by reduction in thermal conductivity via scattering mechanism [7].

Later, nanocomposites were come forward to improve the thermoelectric performance as well as mechanical properties, where the numerous interfaces would severely have scattered the charge carriers and phonons. On the other hand, heterojunction potentials were formed by the incorporation of metallic nano-inclusions there by significant increase in Seebeck coefficient, as well as carrier mobility. However, the dispersed nanoparticles would also affect the electrical conductivity via carrier scattering at interfaces [8]. Zhao et al. reported the ZT of 1.04 in SiC dispersed Bi_2Te_3 poly crystals due to reduction in thermal conductivity via defect scattering mechanism, and improved the mechanical properties such as fracture toughness of 1.34 MPa m$^{1/2}$ [9]. However, the dispersion of nanoceramic (insulating) particles in p-type Bi-Te alloys are not studied yet. In addition, it is quite interesting to investigated the transport properties with addition of insulators in p-type Bi-Te based alloys.

In this research, Ga_2O_3 nanoparticles were selected to be dispersion into the $Bi_{0.5}Sb_{1.5}Te_3$ matrix, because it a wide band gap semiconductor and promotes high inclusion stability with in the host matrix [10]. Besides, the dispersed Ga_2O_3 nanoparticles can enhance the mechanical properties such as hardness, which can benefit for the prevention of cutting loss during the device

* DIVISION OF ADVANCED MATERIALS ENGINEERING AND INSTITUTE FOR RARE METALS, KONGJU NATIONAL UNIVERSITY, CHEONAN, CHUNGNAM, 330-717, KOREA

Corresponding author: hongsj@kongju.ac.kr

fabrication. Also, the dispersion effect of Ga_2O_3 nanoparticles on the microstructure and thermoelectric properties were systematically investigated.

2. Experimental

The elements such as Bismuth (99.999%), Antimony (99.99%), tellurium (99.999%), and Ga_2O_3 used in the study were purchased from Alfa-acer. Initially, p-type $Bi_{0.5}Sb_{1.5}Te_3$ was prepared by gas atomization like our previous studies [11]. The p-type $Bi_{0.5}Sb_{1.5}Te_3$ nanocomposite powders were fabricated by the incorporation of Ga_2O_3 nanoparticles into the gas atomized powders by ball milling (Planetary miller P100), subsequently the nanocomposite powders were consolidated by spark plasma sintering with an axial compressive pressure of 50 MPa at 673 K.

The microstructure and chemical analysis of sintered samples were characterized with field- emission scanning electron microscopy, and energy dispersive spectroscopy (SEM- MIRA LMH II (TESKAN), Czech Republic). The crystal structure was analyzed by X-ray diffraction using monochromatic CuK_α by MiniFlux 600 (Rigaku) system. The relative density, and hardness of the nanocomposites were measured by Archimedes principle, and Vickers hardness tester respectively. The temperature dependence of thermoelectric properties such as Seebeck coefficient, electrical conductivity was measured with the temperature range of 300-400K using thermoelectric power (Seepel, TEP-1000) measurement system. The power factor was calculated from the Seebeck coefficient, and electrical conductivity. The carrier concentration and, hall mobility is measured using Hall-coefficient measurement system (ECOPIA, HMS-3000).

3. Results and discussion

The XRD pattern of the p-type $Bi_{0.5}Sb_{1.5}Te_3$ nanocomposite bulks are illustrated in the Figure 1. It is evident that the all sintered samples were polycrystalline of $Bi_{0.5}Sb_{1.5}Te_3$ phases (JCPDS #49-1713) with rhombohedral crystal structure. The diffraction peaks corresponding to the Ga_2O_3 phases are not observed clearly, which might be due to the small weight percentages of Ga_2O_3 nanoparticles in the matrix. In addition, the intensity of the basal planes is weak, and almost same for all samples, which reveals that no orientation of grains in any special direction is observed [12].

The SEM fracture surfaces of base $Bi_{0.5}Sb_{1.5}Te_3$ sample and nanocomposites are presented in Figure 2. The base $Bi_{0.5}Sb_{1.5}Te_3$ fracture surface in Figure 2(a) shows clean and fine grains distribution with an average grain size of ~4 to 5 μm. Figure 2(b), (c), and (d) shows the fracture surfaces of 2, 4 and 6wt% Ga_2O_3 dispersed $Bi_{0.5}Sb_{1.5}Te_3$ nanocomposites. It is obvious that the grain sizes in nanocomposites are slightly decreases than base $Bi_{0.5}Sb_{1.5}Te_3$ sample. This slight refinement of grain size from 5 to 2 μm might have attributed to the dispersion effect in which the Ga_2O_3 nanoparticles would restrict the grain growth

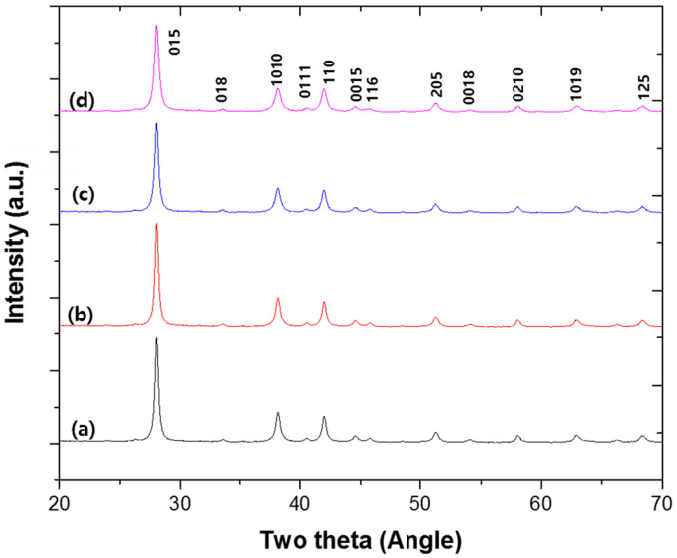

Fig. 1. XRD analysis p-type $Bi_{0.5}Sb_{1.5}Te_3$ with (a) 0 wt% Ga_2O_3, (b) 2 wt% Ga_2O_3 (c) 4 wt% Ga_2O_3, and (d) 6 wt% Ga_2O_3 bulks

during the sintering [13]. The reduction in grain size could be favor for increase in mechanical properties such as hardness, which helps for the preventing the cutting loss during TE device fabrication. In addition, the insets shown in Figure 2(b), (c) and (d) are represent the EDS mapping analysis of nanocomposites and identifies the Ga element distribution in matrix. This results confirm that the Ga_2O_3 nanoparticles existence in the base $Bi_{0.5}Sb_{1.5}Te_3$ matrix. Moreover, Figure 3(a) and 3(b) represents the back-scattered micrographs of 2, and 6 wt% Ga_2O_3 added $Bi_{0.5}Sb_{1.5}Te_3$ nanocomposites. It is evident that the clear visible (black color contrast) Ga_2O_3 nanoparticles are distributed uniformly throughout the surface, and identified with EDS-chemical analysis in Figures 3(c), and (d) respectively. The elemental composition details in spectrum reveals the existence of Ga_2O_3 naoparticles in the $Bi_{0.5}Sb_{1.5}Te_3$ nanocomposites.

The relative density and Vickers hardness of p-type $Bi_{0.5}Sb_{1.5}Te_3$ nanocomposites are listed in Table 1. The relative density is almost 100 % for the base $Bi_{0.5}Sb_{1.5}Te_3$ materials, and its value is decreased upon the dispersion of Ga_2O_3 content in matrix from 2 to 6wt%. The dispersed Ga_2O_3 nanoparticles would give the back force during the sintering which might cause for lower densities in nanocomposites [14]. The Vickers hardness values of $Bi_{0.5}Sb_{1.5}Te_3$ nanocomposites are shown in Table 1. The Vickers hardness value of base $Bi_{0.5}Sb_{1.5}Te_3$ sample is measured of 0.86 GPa, and increased 0.1336 GPa with increasing in Ga_2O_3 content. The improved hardness values are attributed to the slight refinement of the grain size (from ~5 to ~2 μm) in nanocomposites, where fine grains could prevent the cracks propagation upon the indentation load. Also, the distributed Ga_2O_3 nanoparticles could increase the hardness due to dispersion strengthening mechanism. The present work shows improved hardness than other Bi-Te based nanocomposites reported elsewhere [15,16].

The temperature dependence of the Seebeck coefficient of p-type $Bi_{0.5}Sb_{1.5}Te_3$ nanocomposites is presented in Figure 4.

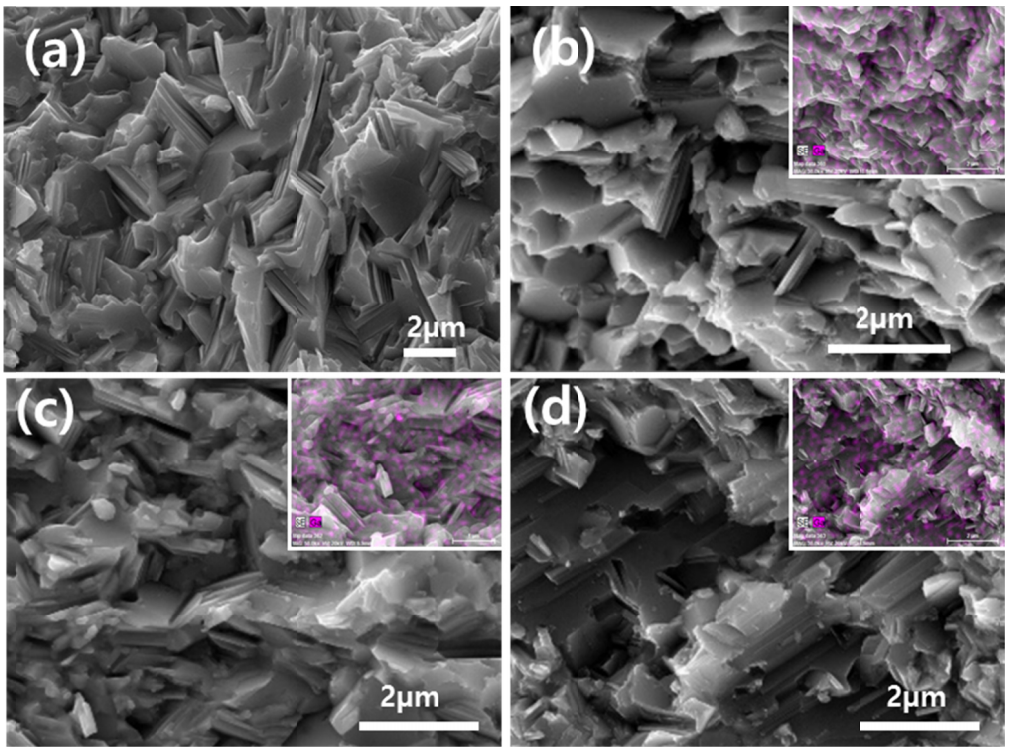

Fig. 2. Fracture surfaces of p-type $Bi_{0.5}Sb_{1.5}Te_3$ with (a) 0 wt% Ga_2O_3, (b) 2 wt% Ga_2O_3 (c) 4 wt% Ga_2O_3 ,and (d) 6 wt% Ga_2O_3 bulks. The inset in (b), (c) and (d) shows the corresponding EDS mapping images

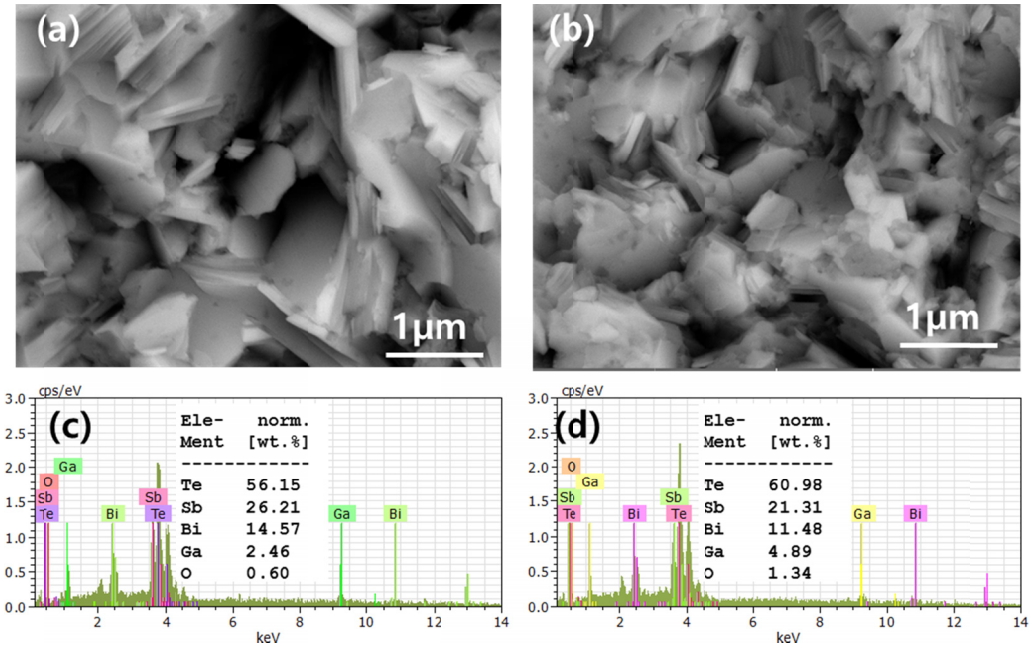

Fig. 3. SEM-BSE micrographs of p-type $Bi_{0.5}Sb_{1.5}Te_3$ with (a) 2 wt% Ga_2O_3, and (d) 6 wt% Ga_2O_3 bulks. (c), and (d) shows the corresponding EDS spectrum with elemental composition content. The distributed Ga_2O_3 are clearly visible (dark color) in the micrographs, and increased content from 2 to 6wt % added Ga_2O_3 in $Bi_{0.5}Sb_{1.5}Te_3$ bulk

TABLE 1

Relative density, Hardness, carrier concentration, hall mobility, reduced fermi level, and bandgap of p-type $Bi_{0.5}Sb_{1.5}Te_3$ nanocomposites

BST/(x-wt%) Ga_2O_3	Relative density (%)	Hardness (GPa)	Carrier concentration, n (10^{19}/cm^3)	Hall mobility, μ (cm^2/ Vs)	Reduced Fermi level, ξ_F (= E_f/k_BT)	Bandgap, Eg ($2e\alpha_{max}T_{max}$)
0	99.7	0.86	1.72	2.68	0.1969	0.175
2	98.6	0.885	0.84	2.79	–0.7004	0.179
4	98.2	0.95	0.92	2.74	–0.7038	0.18
6	97.9	1.336	1.0	2.64	–0.758	0.176

The Seebeck coefficient of all nanocomposites are positive throughout the measured temperature range from 300 to 500 K, indicates that the holes are majority carriers [17]. The Seebeck coefficient of base $Bi_{0.5}Sb_{1.5}Te_3$ specimen is increases with increasing temperature gradually, whereas the nanocomposites show rapid decreasing behavior with temperature which might be due to band structural change (see ξ_F in Table 1) and increase in bandgap (see E_g in Table 1) in upon the dispersion of Ga_2O_3 nanoparticles. It is obvious that the Seebeck coefficient is significantly improved by the incorporation of Ga_2O_3 nanoparticles into the base $Bi_{0.5}Sb_{1.5}Te_3$ sample. The Seebeck coefficient of 192 μV/K is obtained for base $Bi_{0.5}Sb_{1.5}Te_3$ sample, which is eminently improved to ~254 μV/K for the 6wt% of Ga_2O_3 dispersed $Bi_{0.5}Sb_{1.5}Te_3$ nanocomposites. In general, the Seebeck coefficient (α) can expressed in terms of carrier concentration n_c as [18]

$$\alpha = \gamma - ln\, n_c \qquad (1)$$

where γ is the scattering parameter, and nc is the carrier concentration. The measured carrier concentration and hall mobility are shown in the Table 1. It is evident that the carrier concentration of base matrix is about 1.72×10^{19} cm^{-3}, which is dramatically decreased up to ~1.0×10^{19} cm^{-3} upon the dispersion of the Ga_2O_3 nanoparticles in host matrix. K.T. Kim et al argued that the variation in the band structure such a decrease in Fermi energy level (see in Table 1) in nanocomposites would causes for reduction of carrier concentration [17]. Therefore, the rapid decrease in carrier concentration is favorably increases the Seebeck coefficient in the nanocomposites. The present Ga_2O_3 dispersed $Bi_{0.5}Sb_{1.5}Te_3$ nanocomposites show improved Seebeck coefficient than other p-type Bi-Te based nanocomposites [19,20].

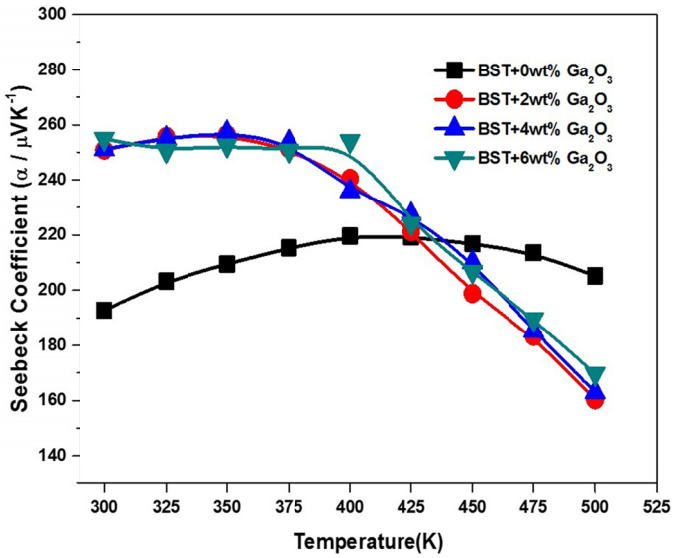

Fig. 4. Temperature dependence of Seebeck coefficient for $Bi_{0.5}Sb_{1.5}Te_3$/(x-wt%)Ga_2O_3 (x = 0, 2, 4 and 6wt%) nanocomposite bulk samples

The temperature dependence of the electrical conductivity of p-type $Bi_{0.5}Sb_{1.5}Te_3$ nanocomposites is presented in Figure 5. The electrical conductivity of all specimens decreased with increasing for temperature indicating a metal -like behavior. It is clearly shown in Figure 5 that the electrical conductivity is severely affected by the dispersion of Ga_2O_3 nanoparticles into base $Bi_{0.5}Sb_{1.5}Te_3$ sample. In addition, the electrical conductivity is decreased with increase in Ga_2O_3 content, which is mainly due to the scattering of carrier at newly formed $Bi_{0.5}Sb_{1.5}Te_3/Ga_2O_3$ interfaces. The electrical conductivity of 822 $\Omega^{-1}cm^{-1}$ obtained for the base $Bi_{0.5}Sb_{1.5}Te_3$ sample, which is ferociously decreased to 345 $\Omega^{-1}cm^{-1}$ for the 6 wt% of Ga_2O_3 dispersed $Bi_{0.5}Sb_{1.5}Te_3$ nanocomposites. In general, the electrical conductivity is given by [16],

$$\sigma = n_c e \mu \qquad (2)$$

where e is the charge of the carrier. The electrical conductivity of the Ga_2O_3 dispersed $Bi_{0.5}Sb_{1.5}Te_3$ nanocomposites is decreased primarily due to the decrease in carrier concentration (see Table 1). However, the carrier mobility is increased for the nanocomposites, which might be balanced with the carrier concentration as per the equation (2).

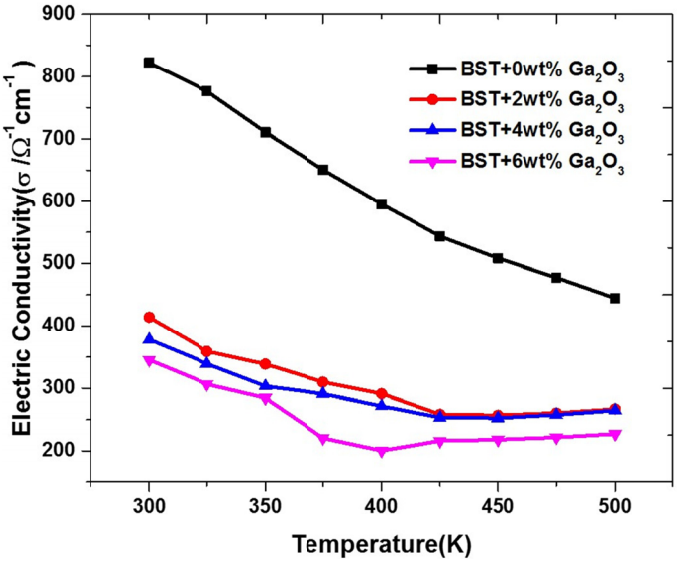

Fig. 5. Temperature dependence of electrical conductivity for $Bi_{0.5}Sb_{1.5}Te_3$/(x-wt%)Ga_2O_3 (x = 0, 2, 4 and 6wt%) nanocomposite bulk samples

The temperature dependence of power factor (PF) values is calculated from the measured Seebeck coefficient, and electrical conductivity (PF = $\alpha^2\sigma$). The calculated powder factor of p-type $Bi_{0.5}Sb_{1.5}Te_3$ nanocomposites are shown in Figure 6. The power factor of all samples are decreases with increasing temperature, which is due to the decreasing behavior of electrical conductivity with temperature. The maximum power factor of 3.24 W/mK^2 is obtained for the base $Bi_{0.5}Sb_{1.5}Te_3$ specimen. However, the PF is decreased in the $Bi_{0.5}Sb_{1.5}Te_3$ nanocomposites due to severe reduction of electrical conductivity. Further studies are underway to balance the electrical conductivity to attain high power factor values.

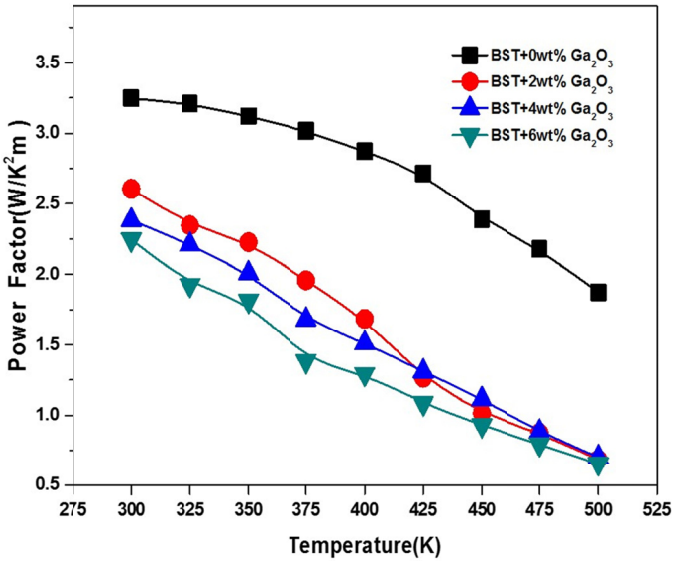

Fig. 6. Temperature dependence of power factor for $Bi_{0.5}Sb_{1.5}Te_3$/(x-wt%)Ga_2O_3 (x = 0, 2, 4 and 6wt%) nanocomposite bulk samples

4. Conclusions

In summary, p-type $Bi_{0.5}Sb_{1.5}Te_3$ based nanocomposite powders were successfully fabricated with dispersing 0wt%, 2 wt%, 4wt%, and 6wt% of Ga_2O_3 nanoparticles into a $Bi_{0.5}Sb_{1.5}Te_3$ host by mechanical milling, subsequently consolidated with spark plasma sintering. The fracture surfaces indicated that the grain sizes were slightly decreases with increasing Ga_2O_3 content in host matrix. The Vickers hardness is remarkably improved for the 6wt% dispersed $Bi_{0.5}Sb_{1.5}Te_3$ nanocomposites. The dispersion effect of Ga_2O_3 on thermoelectric properties of p-type $Bi_{0.5}Sb_{1.5}Te_3$ was systematically investigated. The Seebeck coefficient of $Bi_{0.5}Sb_{1.5}Te_3$ nanocomposites were significantly improved by the Ga_2O_3 nanoparticles dispersion which is mainly due to the decrease in carrier concentration. Besides, the electrical conductivity was decreased. The $Bi_{0.5}Sb_{1.5}Te_3$ nanocomposites show low power factor (2.6 W/mK^2 for 2wt%Ga_2O_3) than base $Bi_{0.5}Sb_{1.5}Te_3$ sample (3.24 W/mK^2) due to their low electrical conductivity.

Acknowledgments

This research (or work) was supported by the Materials and Components Technology Development Program of MOTIE/KEIT, Republic of Korea [10063286, Development of high efficient thermoelectric module with figure of merit (Z) 3.4(X10-3) by using 1.0 kg/batch scale productible polycrystalline thermoelectric material with average figure of merit (ZT) 1.4 and over].

REFERENCES

[1] F.J. DiSalvo, Science **285**, 703 (1999).
[2] D.M. Rowe, Thermoelectric Handbook: Macro to Nano, Taylor & Francis Group, 2006.
[3] Y. Lan, B. Poudel, Y. Ma, D. Wang, M.S. Dresselhaus, G. Chen, Z. Ren, Nano Lett. **9**, 1419 (2009).
[4] H.P. Ha, D.B. Hyun, J.Y. Byun, Y.J. Oh, E.P. Yoon, J. Electronic. Mater **37**, 4691 (2002).
[5] H.S. Kim, B. Madavali, T.J. Eom, C.M. Kim, J.M. Koo, T.H. Lee, S.J. Hong, Arch. Metall. Mater. **60**, 1235 (2015).
[6] B. Poudel, Q. Hao, Y. Ma, Y. Lan, A. Minnich, B. Yu, X. Yan, D. Wang, A. Muto, D. Vashaee, X. Chen, J. Liu, M. S. Dresselhaus, G. Chen, Z. Ren, Science **320**, 634 (2008).
[7] W. Xie, J. He, H.J. Kang, X. Tang, S. Zhu, M. Laver, S. Wang, J.R.D. Copley, C.M. Brown, Q. Zhang, T.M. Tritt, Nano Lett. 10, 3283-3289 (2010).
[8] B. Paul, V.A. Kumar, P. Banerji, J. Appl. Phys. **108**, 064322 (2010).
[9] L.D. Zhao, B.P. Zhang, J.F. Li, M. Zhou, W.S. Liu, J. Liu, J. Alloys Compd. **455**, 259 (2008).
[10] M.D. Santia1, N. Tandon, J.D. Albrecht, Appl. Phys. Lett. **107**, 041907 (2015).
[11] B. Madavali, H.S. Kim, K.H. Lee, I. Yukihiro, F. Gascoin, S.J. Hong, Mater. Des. **112**,485 (2016).
[12] S.J. Hong, B.S. Chun, Mater. Res. Bull. **38**, 599 (2003)
[13] S.J. Jung, S.Y. Park, B.K. Kim, B. Kwon, S.K. Kim, H.H. Park, D.I. Kim, J.Y. Kim, D. Bin Hyun, J.S. Kim, S.H. Baek, Acta Mater. **97**, 68 (2015).
[14] F. Li, X. Huang, Z. Sun, J. Ding, J. Jiang, W. Jiang, L. Chen, J. Alloys Compd. **509**, 4769 (2011).
[15] L.D. Zhao, B.P. Zhang, J.F. Li, et al., M Zhou, W. S. Liu, J. Liu, J. Alloys Comp. **455**, 259 (2008).
[16] H.R. Williams, R.M. Ambrosi, K. Chen, U. Friedman, H. Ning, M.J. Reece, M.C. Robbins, K. Simpson, K. Stephenson, J. Alloys Comp. **626**, 368 (2015).
[17] K.T. Kim, T.S. Lim, G.H. Ha, Reviews on Adv. Mater. Sci. **28**, 196 (2011).
[18] B. Madavali, H.S. Kim, K.H. Lee, H.T. Son, S.J. Hong, Int. J. Appl. Ceram. Technol. **13**, 252 (2016).
[19] K.T. Kim, G.H. Ha, J. Nanometer. **1**, 2013 (2013).
[20] Y.H. Yeo, T.S. Oh, Mater. Res. Bull. **58**, 54 (2014).